Dynamic Behavior of Two Collinear Anti-plane Shear Cracks in a Piezoelectric Layer Bonded to Dissimilar Half Spaces*

Zhen-Gong ZHOU** and Biao WANG**

In this paper, the dynamic behavior of two collinear anti-plane shear cracks in a piezoelectric layer bonded to dissimilar half spaces was investigated for the impermeable crack face conditions. The cracks are vertical to the interfaces of the piezoelectric layer. By means of the Fourier transform, the problem can be solved with two pairs of triple integral equations. These equations are solved by use of the Schmidt method. This process is quite different from that adopted in previously. Numerical examples are provided to show the effect of the geometry of the cracks, the piezoelectric constants of the material and the frequency of the incident wave upon the dynamic stress intensity factor of the cracks.

Key Words: Crack, Stress Waves, Triple Integral Equation, Piezoelectric Materials

1. Introduction

It is well known that piezoelectric materials produce an electric field when deformed and undergo deformation when subjected to an electric field. The coupling nature of piezoelectric materials has attracted wide applications in electric-mechanical and electric devices, such as electric-mechanical actuators, sensors and structures. When subjected to mechanical and electrical loads in service, these piezoelectric materials can fail prematurely due to defects, e.g. cracks, holes, etc., arising during their manufacture process. Therefore, it is of great importance to study the electro-elastic interaction and fracture behaviors of piezoelectric materials. Moreover, it is known that the failure of solids results from the final propagation of the cracks, and in most cases, the unstable growth of the crack is brought about by the external dynamic loads. So, the study of the dynamic fracture mechanics of piezoelectric materials is much more urgent in recent research.

Recently, the dynamic response of piezoelectric materials and the failure modes has attracted more and more attention from many researchers[1]-[5]. A finite crack in an infinite piezoelectric material strip under anti-plane dynamic electromechanical impact was investigated with the well-established integral transform methodology[1]. Axisymmetric vibration of a piezo-composite hollow cylinder was studied in Ref. (2). The dynamic representation formulas and fundamental solutions for piezoelectricity had been proposed earlier in Ref.(3). The dynamic response of a cracked dielectric medium in a uniform electric field was studied in Ref.(4). The scattering of anti-plane shear waves by a finite crack in piezoelectric laminates was also carried out in Ref.(5). Most recently, an infinite piezoelectric ceramic with impermeable crack-face boundary condition under arbitrary electro-mechanical impact was considered in Ref.(6). The response of piezoelectric bodies disturbed by internal electric sources was investigated in Ref. (7). The impermeable boundary condition on the crack surface was widely used in the works[6],[8]-[13]. In particular, control of laminated structures including piezoelectric devices was the subject of research in Refs.(14) - (18). Many piezoelectric devices comprise both piezoelectric and structural layers, and an understanding of the fracture process of piezoelectric structural systems is of great importance in order to ensure the structural integrity of piezoelectric devices[19]-[21].

In the present paper, we consider the anti-plane shear problem for two cracked piezoelectric layer bonded to two half spaces for the impermeable crack face conditions. The traditional concept of linear elastic fracture mechanics is extended to include the piezoelectric effects. The two half spaces have the same properties and the piezoelectric laminate is

* Received 24th August, 2001

** P.O.Box 1247, Center for Composite Materials and Electro-Optics Research Center, Harbin Institute of Technology, Harbin 150001, P.R.China. E-mail: zhouzhg@hope.hit.edu.cn

subjected to combined mechanical and electrical loads. The cracks are situated symmetrically and oriented in the direction vertical to the interfaces of the layer. The interaction between two collinear symmetrical cracks subjects to anti-plane shear waves in piezoelectric layer bonded to two half spaces was investigated using some different approach by a new method, namely Schmidt method[22]. It is a simple and convenient method for solving this problem. Fourier transform is applied and a mixed boundary value problem is reduced to two pairs of triple integral equations. In solving the triple integral equations, the crack surface displacement and electric potential are expanded in a series using Jacobi's polynomials. This process is quite different from those adopted as mentioned above and Refs.(23) - (31). The form of solution is easy to understand. Numerical calculations are carried out for the stress intensity factors.

2. Formulation of the Problem

Consider a piezoelectric layer that is sandwiched between two elastic half planes with an elastic stiffness constant c_{44}^E. Quantities in the half spaces will subsequently be designated by superscript E. The piezoelectric materials layer of thickness $2h$ contains two impermeable cracks of length $l=1-b$ that are vertical to the interfaces, as shown in Fig. 1. $2b$ is the distance between the cracks (The solution of the piezoelectric layer of width $2h$ containing two collinear Griffith cracks of length $a-b$ can easily be obtained by a simple change in the numerical values of the present paper. $a>b>0$). The piezoelectric boundary-value problem for anti-plane shear is considerably simplified if we consider only the out-of-plane displacement and the in-plane electric fields. Let ω be the circular frequency of the incident wave. In what follows, the time dependence of all field quantities assumed to be of the form $\exp(-j\omega t)$ will be suppressed but understood. We further suppose that the two faces of the crack do not come into contact during vibrations. The constitutive equations can be written as

$$\tau_{zk}=c_{44}w_{,k}+e_{15}\phi_{,k} \quad (1)$$

$$D_k=e_{15}w_{,k}-\varepsilon_{11}\phi_{,k} \quad (2)$$

$$\tau_{xz}^E=c_{44}^E w_{,x}^E \quad (3)$$

$$\tau_{yz}^E=c_{44}^E w_{,y}^E \quad (4)$$

where τ, D_k $(k=x, y)$ are the anti-plane shear stress and in-plane electric displacement, respectively. c_{44}, e_{15}, ε_{11} are the shear modulus, piezoelectric coefficient and dielectric parameter, respectively. w and ϕ are the mechanical displacement and electric potential. τ_{xz}^E, τ_{yz}^E and w^E are the shear stress, and the displacement in the half elastic spaces, respectively. The anti-plane governing equations are[5]:

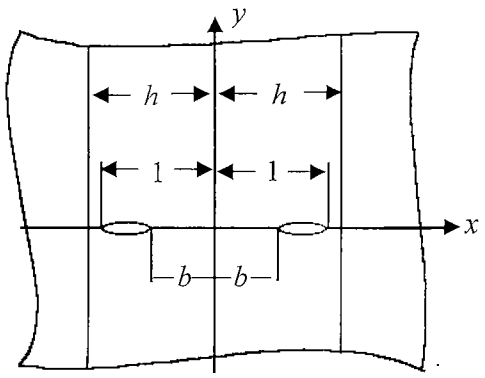

Fig. 1 Cracks in a piezoelectric layer body under anti-plane shear

$$c_{44}\nabla^2 w+e_{15}\nabla^2\phi=\rho\partial^2 w/\partial t^2 \quad (5)$$

$$e_{15}\nabla^2 w-\varepsilon_{11}\nabla^2\phi=0 \quad (6)$$

$$\nabla^2 w^E=\rho^E\partial^2 w^E/\partial t^2 \quad (7)$$

where $\nabla^2=\partial^2/\partial x^2+\partial^2/\partial y^2$ is the two dimensional Laplace operator. ρ is the mass density of the piezoelectric materials. ρ^E is the mass density of the elastic materials. Body force, other than inertia, and the free charge are ignored in the present work. Because of the assumed symmetry in geometry and loading, it is sufficient to consider the problem for $0\leq x<\infty$, $0\leq y<\infty$ only.

A Fourier transform is applied to Eqs.(5), (6) and (7). Assume that the solutions are

$$w(x, y, t)=\frac{2}{\pi}\int_0^\infty A_1(s)^{-\gamma_1 y}\cos(sx)ds+\frac{2}{\pi}\int_0^\infty A_2(s)\cosh(\gamma_1 x)\sin(sy)ds \quad (8)$$

$$w^E(x, y, t)=\frac{2}{\pi}\int_0^\infty C(s)e^{-\gamma_2 x}\sin(sy)ds \quad (9)$$

where $\gamma_1=\sqrt{s^2-(\omega/c_{SH})^2}$, $c_{SH}=\sqrt{\mu/\rho}$, $\mu=c_{44}+\frac{e_{15}^2}{\varepsilon_{11}}$, $\gamma_2=\sqrt{s^2-(\omega/c_{SH}^E)^2}$, $c_{SH}^E=\sqrt{c_{44}^E/\rho^E}$, $A_1(s)$, $A_2(s)$ and $C(s)$ are unknown functions, and a superposed bar indicates the Fourier transform throughout the paper, e.g.,

$$\bar{f}(s)=\int_{-\infty}^{\infty}f(x)e^{-isx}dx \quad (10)$$

Inserting Eq.(8) into Eq.(6), it can be assumed that

$$\phi(x, y, t)-\frac{e_{15}}{\varepsilon_{11}}w(x, y, t)=\frac{2}{\pi}\int_0^\infty B_1(s)e^{-sy}\cos(sx)ds+\frac{2}{\pi}\int_0^\infty B_2(s)\cosh(sx)\sin(sy)ds \quad (11)$$

where $B_1(s)$ and $B_2(s)$ are unknown functions.

As discussed in Refs.(4), (5), (32), the boundary conditions of the present problem are:

$$\tau_{yz}(x, 0, t)=-\tau_0, \quad b\leq|x|\leq 1 \tag{12}$$
$$D_y(x, 0, t)=-D_0, \quad b\leq|x|\leq 1 \tag{13}$$
$$w(x, 0, t)=\phi(x, 0, t)=0, \quad |x|<b, \ |x|>1 \tag{14}$$
$$\tau_{xz}(\pm h, y, t)=\tau_{xz}^{E}(\pm h, y, t), \tag{15}$$
$$w(\pm h, y, t)=w^{E}(\pm h, y, t) \tag{16}$$
$$D_x(\pm h, y, t)=0 \tag{17}$$
$$w(x, y, t)=w^{E}(x, y, t)=\phi(x, y, t)=0, \text{ for } \sqrt{x^2+y^2}\rightarrow\infty \tag{18}$$

In this paper, the wave is vertically incident and we only consider positive τ_0 and D_0. The boundary conditions can be applied to yield two pairs of triple integral equations:

$$\frac{2}{\pi}\int_0^{\infty}A_1(s)\cos(sx)ds=0, \quad 0\leq x<b, \ h\geq x>1 \tag{19}$$
$$\frac{2}{\pi}\int_0^{\infty}\gamma_1 A_1(s)\cos(sx)ds=\frac{2}{\pi}\int_0^{\infty}sA_2(s)\cosh(\gamma_1 x)ds+\frac{1}{\mu}\left(\tau_0+\frac{e_{15}D_0}{\varepsilon_{11}}\right), \ b\leq x\leq 1 \tag{20}$$

and

$$\frac{2}{\pi}\int_0^{\infty}B_1(s)\cos(sx)ds=0, \quad 0\leq x<b, \ h\geq x>1 \tag{21}$$
$$\frac{2}{\pi}\int_0^{\infty}sB_1(s)\cos(sx)ds=\frac{2}{\pi}\int_0^{\infty}sB_2(s)\cosh(sx)ds-\frac{D_0}{\varepsilon_{11}}, \ b\leq x\leq 1 \tag{22}$$

The relationships between the functions $A_1(s)$, $A_2(s)$, $B_1(s)$, $B_2(s)$ and $C(s)$ are obtained by applying the Fourier sine transform[33] to Eqs.(15) - (17):

$$A_2(t)[\gamma_1\sinh(\gamma_1 h)+\mu_1\gamma_2\cosh(\gamma_1 h)]=\frac{2t}{\pi}\int_0^{\infty}\frac{\sin(sh)s-\gamma_2(t)\mu_1\cos(sh)}{\gamma_1^2(s)+t^2}A_1(s)ds \tag{23}$$
$$C(t)e^{-\gamma_2 h}[\gamma_1\sinh(\gamma_1 h)+\mu_1\gamma_2\cosh(\gamma_1 h)]=\frac{2t}{\pi}\int_0^{\infty}\frac{\cosh[\gamma_1(t)h]\sin(sh)s+\gamma_1(t)\sinh[\gamma_1(t)h]\cos(sh)}{\gamma_1^2(s)+t^2}A_1(s)ds \tag{24}$$
$$B_2(t)\sinh(th)=\frac{2}{\pi}\int_0^{\infty}\frac{s}{s^2+t^2}B_1(s)\sin(sh)ds, \ \mu_1=\frac{c_{44}^{E}}{\mu} \tag{25}$$

To determine the unknown functions $A_1(s)$, $B_1(s)$, the above two pairs of triple integral Eqs.(19) - (22) must be solved.

3. Solution of the Triple Integral Equation

The Schmidt method[22] is used to solve the triple integral Eqs.(19) - (22). The displacement w and the electric potential ϕ can be represented by the following series:

$$w(x, 0, t)=\sum_{n=0}^{\infty}a_n P_n^{\left(\frac{1}{2},\frac{1}{2}\right)}\left(\frac{x-\frac{1-b}{2}}{\frac{1-b}{2}}\right)\left(1-\frac{\left(x-\frac{1+b}{2}\right)^2}{\left(\frac{1-b}{2}\right)^2}\right)^{\frac{1}{2}}, \quad \text{for } b\leq x\leq 1, \ y=0 \tag{26}$$
$$w(x, 0, t)=0, \quad \text{for } x<b, \ x>1, \ y=0 \tag{27}$$
$$\phi(x, 0, t)=\sum_{n=0}^{\infty}b_n P_n^{\left(\frac{1}{2},\frac{1}{2}\right)}\left(\frac{x-\frac{1+b}{2}}{\frac{1-b}{2}}\right)\left(1-\frac{\left(x-\frac{1+b}{2}\right)^2}{\left(\frac{1-b}{2}\right)^2}\right)^{\frac{1}{2}}, \quad \text{for } b\leq x\leq 1, \ y=0 \tag{28}$$
$$\phi(x, 0, t)=0, \text{ for } x<b, \ x>1, \ y=0 \tag{29}$$

where a_n and b_n are unknown coefficients to be determined and $P_n^{(1/2,1/2)}(x)$ is a Jacobi polynomial[33]. The Fourier transformation of Eqs.(26) and (28) is[34]:

$$A_1(s)=\bar{w}(s, 0, t)=\sum_{n=0}^{\infty}a_n Q_n G_n(s)\frac{1}{s}J_{n+1}\left(s\frac{1-b}{2}\right) \tag{30}$$

$$B_1(s)=\bar{\phi}(s, 0, t)-\frac{e_{15}}{\varepsilon_{11}}\bar{w}(s, 0)=\sum_{n=0}^{\infty}\left(b_n-\frac{e_{15}}{\varepsilon_{11}}a_n\right)Q_n G_n(s)\frac{1}{s}J_{n+1}\left(s\frac{1-b}{2}\right) \tag{31}$$
$$Q_n=2\sqrt{\pi}\frac{\Gamma\left(n+1+\frac{1}{2}\right)}{n!} \tag{32}$$
$$G_n(s)=\begin{cases}(-1)^{\frac{n}{2}}\cos\left(s\frac{1+b}{2}\right), & n=0, 2, 4, 6, \cdots\\ (-1)^{\frac{n+1}{2}}\sin\left(s\frac{1+b}{2}\right), & n=1, 3, 5, 7, \cdots\end{cases} \tag{33}$$

where $\Gamma(x)$ and $J_n(x)$ are the Gamma and Bessel functions, respectively.

Substituting Eqs.(30) and (31) into Eqs.(19) - (22), respectively, the Eqs.(19) and (21) can be automatically satisfied, respectively. Then the remaining Eqs.(20) and (22) reduce to the form after integration with respect to x in $[b, x]$, respectively.

$$\sum_{n=0}^{\infty}a_n Q_n\int_0^{\infty}s^{-1}[f(s)+1]G_n(s)J_{n+1}\left(s\frac{1-b}{2}\right)[\sin(sx)-\sin(sb)]ds=\frac{\pi}{2\mu}\tau_0(1+\lambda)(x-b)+\frac{2}{\pi}\sum_{n=0}^{\infty}a_n Q_n\times\int_0^{\infty}\frac{s^2[\sinh(\gamma_1 x)-\sinh(\gamma_1 b)]}{g_1(s)}ds\times\int_0^{\infty}G_n(\eta)J_{n+1}\left(\eta\frac{1-b}{2}\right)$$

$$\times\frac{\eta\sin(\eta h)-\gamma_2(s)\mu_1\cos(\eta h)}{g_2(s,\eta)\eta}d\eta \tag{34}$$

$$\sum_{n=0}^{\infty}\left(b_n-\frac{e_{15}}{\varepsilon_{11}}a_n\right)Q_n\int_0^{\infty}s^{-1}G_n(s)J_{n+1}\left(s\frac{1-b}{2}\right)\times[\sin(sx)-\sin(sb)]ds$$
$$=-\frac{\pi D_0}{2\varepsilon_{11}}(x-b)+\frac{2}{\pi}\sum_{n=0}^{\infty}\left(b_n-\frac{e_{15}}{\varepsilon_{11}}a_n\right)Q_n\times\int_0^{\infty}\frac{\sinh(sx)-\sinh(sb)}{\sinh(sh)}ds\times\int_0^{\infty}G_n(\eta)J_{n+1}\left(\eta\frac{1-b}{2}\right)\frac{\sin(\eta h)}{(\eta^2+s^2)}d\eta \tag{35}$$

where $\lambda=\frac{e_{15}D_0}{\varepsilon_{11}\tau_0}$, $f(s)=\frac{\gamma_1-s}{s}$, $g_1(s)=\gamma_1[\gamma_1\sinh(\gamma_1 h)+\mu_1\gamma_2\cosh(\gamma_1 h)]$, $g_2(s,\eta)=\gamma_1^2(\eta)+s^2$.

For a large s, the integrands of the double semi-infinite integral in Eqs.(34) and (35) almost all have exponential forms except for the singularities in the integrands of the integrals in Eq.(34). The zero points of the functions $g_1(s)$ and $g_2(s,\eta)$ are poles of the integrals in Eq.(34). The technique merely deforms the contour of integration below the real s-axis so that no poles occur on the path of integration. These zero points of $g_1(s)$ and $g_2(s,\eta)$ not only depend on the width of piezoelectric layer and the frequency of the incident wave, but also depend on the properties of the materials. These poles represent the addition of a free wave solution that will ensure that the scattering wave solution does not contain standing waves[35]. Note that the integrals in Eq.(34) will also have principle value integrals. Thus the double semi-infinite integral in the Eqs.(34) and (35) can be evaluated numerically by Filon's method[36]. The semi-infinite integral in Eqs.(34) and (35) can be modified as Ref.(33)

$$\int_0^{\infty}\frac{1}{s}[1+f(s)]J_{n+1}\left(s\frac{1-b}{2}\right)\cos\left(s\frac{1+b}{2}\right)\sin(sx)ds$$
$$=\frac{1}{2(n+1)}\times\left\{\frac{\left(\frac{1-b}{2}\right)^{n+1}\sin\left(\frac{(n+1)\pi}{2}\right)}{\left\{x+\frac{1+b}{2}+\sqrt{\left(x+\frac{1+b}{2}\right)^2-\left(\frac{1-b}{2}\right)^2}\right\}^{n+1}}-\sin\left[(n+1)\sin^{-1}\left(\frac{1+b-2x}{1-b}\right)\right]\right\}+\int_0^{\infty}\frac{1}{s}f(s)J_{n+1}\left(s\frac{1-b}{2}\right)\cos\left(s\frac{1+b}{2}\right)\sin(sx)ds \tag{36}$$

$$\int_0^{\infty}\frac{1}{s}[1+f(s)]J_{n+1}\left(s\frac{1-b}{2}\right)\sin\left(s\frac{1+b}{2}\right)\sin(sx)ds$$
$$=\frac{1}{2(n+1)}\left\{\cos\left[(n+1)\sin^{-1}\left(\frac{1+b-2x}{1-b}\right)\right]-\frac{\left(\frac{1-b}{2}\right)^{n+1}\cos\left(\frac{(n+1)\pi}{2}\right)}{\left\{x+\frac{1+b}{2}+\sqrt{\left(x+\frac{1+b}{2}\right)^2-\left(\frac{1-b}{2}\right)^2}\right\}^{n+1}}\right\}+\int_0^{\infty}\frac{1}{s}f(s)J_{n+1}\left(s\frac{1-b}{2}\right)\sin\left(s\frac{1+b}{2}\right)\sin(sx)ds \tag{37}$$

For a large s, the integrands of the semi-infinite integral in the Eqs.(36) and (37) almost all $1/s^2$. Thus the semi-infinite integral in Eqs.(34) and (35) can be evaluated directly. Equations (34) and (35) can now be solved for the coefficients a_n and b_n by the Schmidt method[22]. For brevity, the Eq.(34) can be rewritten as (the Eq.(35) can be solved using a similar method as following)

$$\sum_{n=0}^{\infty}a_nE_n(x)=U(x),\quad b<x<1 \tag{38}$$

where $E_n(x)$ and $U(x)$ are known functions and coefficients a_n are unknown and will be determined. A set of functions $P_n(x)$ which satisfy the orthogonality conditions

$$\int_b^1P_m(x)F_n(x)dx=N_n\delta_{mn},\quad N_n=\int_b^1P_n^2(x)dx \tag{39}$$

can be constructed from the function, $E_n(x)$, such that

$$P_n(x)=\sum_{i=0}^{n}\frac{M_{in}}{M_{nn}}E_i(x) \tag{40}$$

where M_{ij} is the cofactor of the element d_{ij} of D_n, which is defined as

$$D_n=\begin{bmatrix}d_{00}, d_{01}, d_{02}, \cdots, d_{0n}\\ d_{10}, d_{11}, d_{12}, \cdots, d_{1n}\\ d_{20}, d_{21}, d_{22}, \cdots, d_{2n}\\ \cdots\cdots\cdots\\ \cdots\cdots\cdots\\ \cdots\cdots\cdots\\ d_{n0}, d_{n1}, d_{n2}, \cdots, d_{nm}\end{bmatrix},\quad d_{ij}=\int_b^1E_i(x)E_j(x)dx \tag{41}$$

Using Eqs.(38) - (41), we obtain

$$a_n=\sum_{j=n}^{\infty}q_j\frac{M_{nj}}{M_{jj}} \tag{42}$$

with $$q_j=\frac{1}{N_j}\int_b^1U(x)P_j(x)dx \tag{43}$$

4. Intensity Factors

We can determine the entire stress field and the electric displacement from coefficients a_n and b_n. It is of importance in fracture mechanics to determine stress τ_{yz} and the electric displacement D_y in the vicinity of the crack's tips. τ_{yz} and D_y along the crack line can be expressed respectively as

$$\tau_{yz}(x,0,t)=-\frac{2\mu}{\pi}\sum_{n=0}^{\infty}a_nQ_n\Big\{\int_0^{\infty}[f(s)+1]G_n(s)J_{n+1}\Big(s\frac{1-b}{2}\Big)\cos(xs)ds$$
$$-\frac{2}{\pi}\int_0^{\infty}\frac{\cosh(\gamma_1 x)s^2}{[\gamma_1\sinh(\gamma_1 h)+\mu_1\gamma_2\cosh(\gamma_1 h)]}ds\int_0^{\infty}G_n(\eta)J_{n+1}\Big(\eta\frac{1-b}{2}\Big)\frac{\eta\sin(\eta h)-\gamma_2(s)\mu_1\cos(\eta h)}{[\gamma_1^2(\eta)+s^2]\eta}d\eta\Big\}$$
$$-\frac{2e_{15}}{\pi}\sum_{n=0}^{\infty}\Big(b_n-\frac{e_{15}}{\varepsilon_{11}}a_n\Big)Q_n\Big[\int_0^{\infty}G_n(s)J_{n+1}\Big(s\frac{1-b}{2}\Big)\cos(xs)ds-\frac{2}{\pi}\int_0^{\infty}\frac{\cosh(sx)s}{\sinh(sh)}ds$$
$$\times\int_0^{\infty}G_n(\eta)J_{n+1}\Big(\eta\frac{1-b}{2}\Big)\frac{\sin(\eta h)}{(\eta^2+s^2)}d\eta\Big] \tag{44}$$

$$D_y(x,0,t)=\frac{2}{\pi}\sum_{n=0}^{\infty}(\varepsilon_{11}b_n-e_{15}a_n)Q_n\Big[\int_0^{\infty}G_n(s)J_{n+1}\Big(s\frac{1-b}{2}\Big)\cos(xs)ds-\frac{2}{\pi}\int_0^{\infty}\frac{\cosh(sx)s}{\sinh(sh)}ds$$
$$\times\int_0^{\infty}G_n(\eta)J_{n+1}\Big(\eta\frac{1-b}{2}\Big)\frac{\sin(\eta h)}{(\eta^2+s^2)}d\eta\Big] \tag{45}$$

Observing the expression in Eqs. (44) and (45), the singular portion of the stress field and the singular portion of electric displacement can be obtained respectively from the relationships[33]:

$$\cos\Big(s\frac{1+b}{2}\Big)\cos(sx)=\frac{1}{2}\Big\{\cos\Big[s\Big(\frac{1+b}{2}-x\Big)\Big]+\cos\Big[s\Big(\frac{1+b}{2}+x\Big)\Big]\Big\}$$
$$\sin\Big(s\frac{1+b}{2}\Big)\cos(sx)=\frac{1}{2}\Big\{\sin\Big[s\Big(\frac{1+b}{2}-x\Big)\Big]+\sin\Big[s\Big(\frac{1+b}{2}+x\Big)\Big]\Big\}$$

$$\int_0^{\infty}J_n(sa)\cos(bs)ds=\begin{cases}\dfrac{\cos[n\sin^{-1}(b/a)]}{\sqrt{a^2-b^2}}, & a>b\\ -\dfrac{a^n\sin(n\pi/2)}{\sqrt{b^2-a^2}[b+\sqrt{b^2-a^2}]^n}, & b>a\end{cases}$$

$$\int_0^{\infty}J_n(sa)\sin(bs)ds=\begin{cases}\dfrac{\sin[n\sin^{-1}(b/a)]}{\sqrt{a^2-b^2}}, & a>b\\ \dfrac{a^n\cos(n\pi/2)}{\sqrt{b^2-a^2}[b+\sqrt{b^2-a^2}]^n}, & b>a\end{cases}$$

The singular portion of the stress field and the singular portion of electric displacement can be expressed respectively as following

$$\tau=-\frac{1}{\pi}\sum_{n=0}^{\infty}(c_{44}a_n+e_{15}b_n)Q_nH_n(b,x) \tag{46}$$

$$D=\frac{1}{\pi}\sum_{n=0}^{\infty}(\varepsilon_{11}b_n-e_{15}a_n)Q_nH_n(b,x) \tag{47}$$

where $H_n(b,x)=-F_1(b,x,n)$, $n=0,1,2,3,4,5,\cdots$ (for $0<x<b$),

$H_n(b,x)=(-1)^{n+1}F_2(b,x,n)$, $n=0,1,2,3,4,5,\cdots$ (for $1<x$),

$$F_1(b,x,n)=\frac{2(1-b)^{n+1}}{\sqrt{(1+b-2x)^2-(1-b)^2}[1-b-2x+\sqrt{(1+b-2x)^2-(1-b)^2}]^{n+1}}$$

$$F_2(b,x,n)=\frac{2(1-b)^{n+1}}{\sqrt{(2x-1-b)^2-(1-b)^2}[2x-1-b+\sqrt{(2x-1-b)^2-(1-b)^2}]^{n+1}}$$

At the left tip of the right crack, we obtain the stress intensity factor K_L as

$$K_L=\lim_{x\to b^-}\sqrt{2\pi(b-x)}\cdot\tau=\sqrt{\frac{2}{\pi(1-b)}}\sum_{n=0}^{\infty}(c_{44}a_n+e_{15}b_n)Q_n \tag{48}$$

At the right tip of the right crack, we obtain the stress intensity factor K_R as

$$K_R=\lim_{x\to 1^+}\sqrt{2\pi(x-1)}\cdot\tau=\sqrt{\frac{2}{\pi(1-b)}}\sum_{n=0}^{\infty}(-1)^n(c_{44}a_n+e_{15}b_n)Q_n \tag{49}$$

At the left tip of the right crack, we obtain the electric displacement intensity factor K_L^D as

$$K_L^D=\lim_{x\to b^-}\sqrt{2\pi(b-x)}\cdot D=\sqrt{\frac{2}{\pi(1-b)}}\sum_{n=0}^{\infty}(e_{15}a_n-\varepsilon_{11}b_n)Q_n \tag{50}$$

At the right tip of the right crack, we obtain the electric displacement intensity factor K_R^D as

$$K_R^D=\lim_{x\to 1^+}\sqrt{2\pi(x-1)}\cdot D=\sqrt{\frac{2}{\pi(1-b)}}\times\sum_{n=0}^{\infty}(-1)^n(e_{15}a_n-\varepsilon_{11}b_n)Q_n \tag{51}$$

5. Numerical Calculations and Discussion

This section presents numerical results of several representative problems. From the references[37]-[40], it can be seen that the Schmidt method is performed satisfactorily if the first ten terms of the infinite series of Eq. (38) are obtained. The solution of two collinear cracks of arbitrary length a-b can easily be obtained by a simple change in the numerical values of the present paper ($a>b>0$), i.e., it can use the results of the collinear cracks of length $1-b/a$ and the strip width h/a in the present paper. The solution of this paper is suitable for the arbitrary length two collinear cracks in the piezoelectric layer bonded to dissimilar

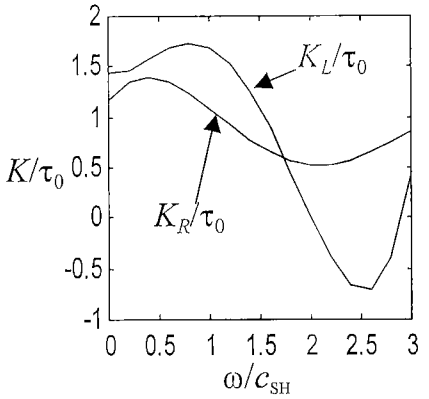

Fig. 2 Stress intensity factor versus ω/c_{SH} for $\lambda=0.2$, $h=1.1$, $b=0.1$ (Aluminum/PZT-4/Aluminum)

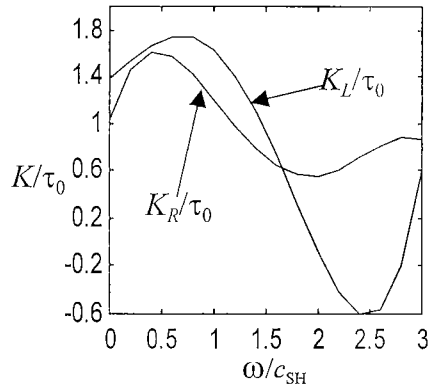

Fig. 3 Stress intensity factor versus ω/c_{SH} for $\lambda=0.2$, $h=2.0$, $b=0.1$ (Aluminum/PZT-4/Aluminum)

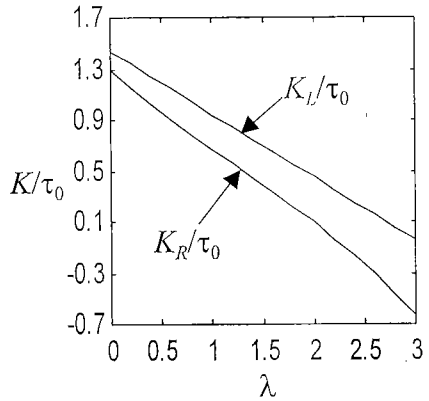

Fig. 4 Stress intensity factor versus λ for $h=1.1$, $\omega/c_{SH}=0.5$, $b=0.1$ (Aluminum/PZT-4/Aluminum)

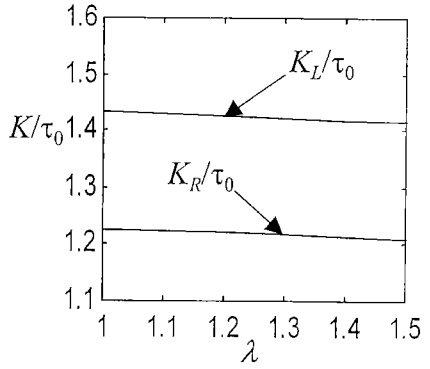

Fig. 5 Stress intensity factor versus λ for $h=4.0$, $\omega/c_{SH}=0.5$, $b=0.1$ (Aluminum/PZT-4/Aluminum)

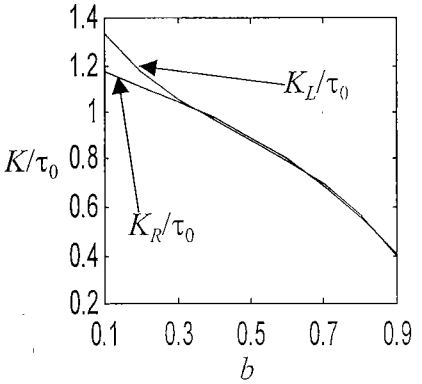

Fig. 6 Stress intensity factor versus b for $\omega/c_{SH}=0.5$, $h=1.1$, $\lambda=0.2$ (Aluminum/PZT-4/Aluminum)

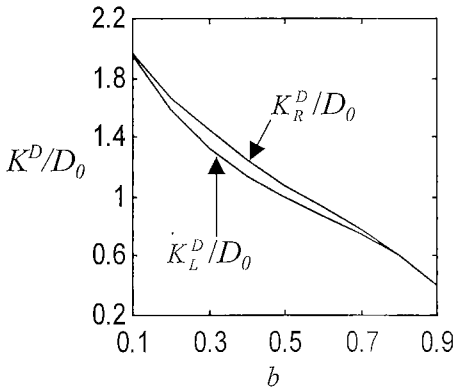

Fig. 7 Electric displacement intensity factor versus b for $\omega/c_{SH}=0.5$, $h=1.1$, $\lambda=0.2$ (Aluminum/PZT-4/Aluminum)

half spaces. All applications were focused on two cracked piezoelectric layer bonded to half planes. The piezoelectric layer is assumed to be the commercially available piezoelectric PZT-4 or PZT-5H, and the half planes are either aluminum or epoxy. The material constants of PZT-4 are $c_{44}=2.56\,(\times10^{10}\,\mathrm{N/m^2})$, $e_{15}=12.7\,(\mathrm{c/m^2})$, $\varepsilon_{11}=64.6\,(\times10^{-10}\,\mathrm{c/Vm^2})$, $\rho=7\,500\,\mathrm{kg/m^3}$, respectively. The material constants of PZT-5H are $c_{44}=2.3\,(\times10^{10}\,\mathrm{N/m^2})$, $e_{15}=17.0\,(\mathrm{c/m^2})$, $\varepsilon_{11}=150.4\,(\times10^{-10}\,\mathrm{c/Vm^2})$, $\rho=7\,500\,\mathrm{kg/m^3}$. The material constants of aluminum are $c_{44}^E=2.65\,(\times10^{10}\,\mathrm{N/m^2})$ and $\rho=2\,706\,\mathrm{kg/m^3}$. The material constants of epoxy are $c_{44}^E=0.176\,(\times10^{10}\,\mathrm{N/m^2})$ and $\rho=1\,600\,\mathrm{kg/m^3}$. The results of the present paper are shown in Figs. 2 to 13, respectively. Form the results, the following observations are very significant:

(i) The results show that the dynamic field will

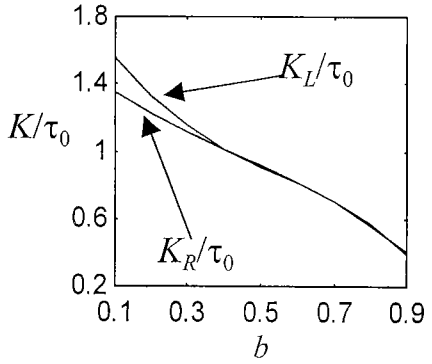

Fig. 8 Stress intensity factor versus b for $\omega/c_{SH}=0.5$, $h=3.0$, $\lambda=0.2$ (Aluminum/PZT-4/Aluminum)

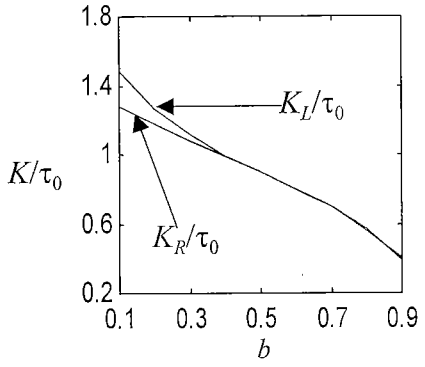

Fig. 9 Electric intensity factor versus b for $\omega/c_{SH}=0.5$, $h=5.0$, $\lambda=0.2$ (Aluminum/PZT-4/Aluminum)

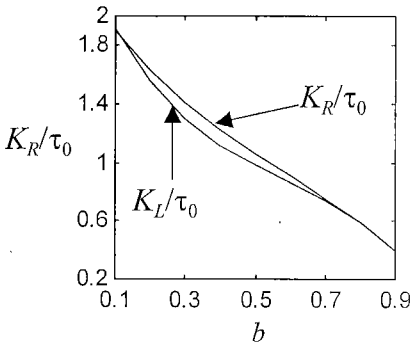

Fig. 10 Stress intensity factor versus b for $h=1.1$, $\omega/c_{SH}=0.5$, $\lambda=0.2$ (Aluminum/PZT-4/Aluminum)

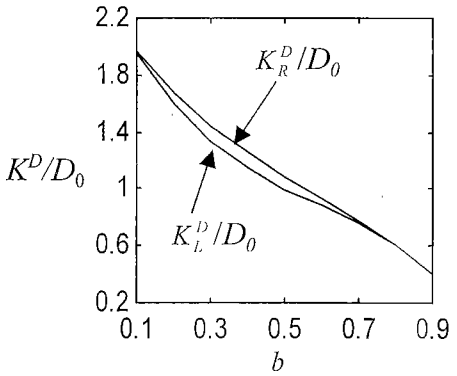

Fig. 11 Electric displacement intensity factor versus b for $h=1.1$, $\omega/c_{SH}=0.5$, $\lambda=0.2$ (Epoxy/PZT-4/Epoxy)

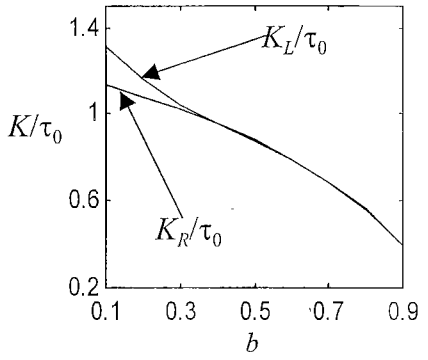

Fig. 12 Stress intensity factor versus b for $h=1.1$, $\omega/c_{SH}=0.5$, $\lambda=0.2$ (Aluminum/PZT-5H/Aluminum)

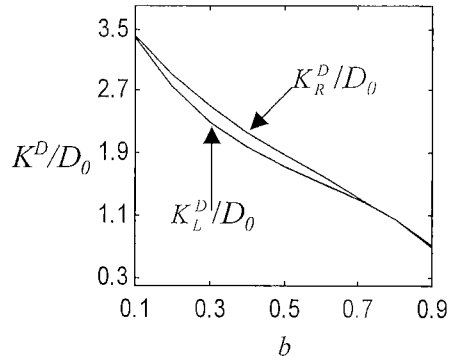

Fig. 13 Electric displacement intensity factor versus b for $h=1.1$, $\omega/c_{SH}=0.5$, $\lambda=0.2$ (Aluminum/PZT-5H/Aluminum)

impede or enhance crack propagation in a piezoelectric material at different stages of dynamic electromechanical load. The dynamic stress intensity factors not only depend on the crack length, the electric loading and the frequency of the incident wave, but also depend on the properties of the materials. Therefore the crack extension may be retarded by adjusting the loading conditions, parameters of the materials and the incident wave frequency.

(ii) The dynamic stress intensity factors tend to increase with the frequency reaching a peak and then to decrease in magnitude. However, when the frequency $\omega/c_{SH}>2.5$, the dynamic stress intensity factors tend to increase with the frequency again as shown in Figs. 2 and 3. This phenomenon is brought up by the free wave. Here, the free wave is created by the singularities in the integrands of the integrals in Eq. (34). So the stress field can reach the minimum value by changing the frequency of the incident waves.

(iii) The stress intensity factor becomes small with increase of the electric loading as shown in Figs.

4 and 5; in other words, the electric field will reduce the magnitude of the stress intensity factor. This is due to the coupling between the electric and the mechanical fields. The intensity of the stress field can be reduced by increasing the intensity of the electric field as shown in Figs. 4 and 5.

(iv) The stress intensity factors at the inner crack tips are bigger than those at the out crack tips for $h \geq 3.0$ as shown in Fig. 9. However, the stress intensity factors at the inner and outer crack tips are almost overlapped $h=1.1$, $b \geq 0.5$ as shown in Figs. 6, 8, 9 and 12 except for in Fig. 10. In Fig. 10, K_R/τ_0 is bigger than K_R/τ_0 for $0.1 \leq b \leq 0.7$. These phenomena may be caused by the coupling between the mechanical and the electric field and by the free wave as mentioned in (ii). Another reason, the material constant c_{44}^E of Epoxy is very small. For the electric displacement intensity factors, K_R^D/D_0 is bigger than K_L^D/D_0 for $0.1 \leq b \leq 0.4$. These phenomena may be also caused by the same reasons as mentioned above.

(v) The dynamic response of the electric field is independent of the external mechanical load. It is coherent with the applied dynamic electric load.

(vi) The behavior of the stress and the electric field near the crack tips will stay steady with increasing of the width of piezoelectric material layer as shown in Fig. 5.

(vii) The effects of the two collinear cracks decrease with increasing of the distance between the two collinear cracks as shown in Figs. 6 to 11. The increasing of the crack density will enhance the crack initiation in a piezoelectric material.

6. Conclusions

We developed an electro-elastic fracture mechanics analysis to determine the singular stress and electric fields near the crack tip for a piezoelectric laminate having two finite cracks vertical to the interface under longitudinal shear waves for the impermeable crack face conditions. The traditional concept of linear elastic fracture mechanics is extended to include the piezoelectric effects and the results are expressed in terms of the dynamic stress intensity factors. Furthermore, the effect of the geometry of the interacting cracks, the material constants and the frequency of the incident wave upon the dynamic stress intensity factors of the crack are examined and their influence discussed. This study reveals the importance of the electro-mechanical coupling terms upon the resulting of dynamic stress intensity factors.

Acknowledgements

The authors are grateful for financial support from the Post Doctoral Science Foundation of Hei Long Jiang Province, the Natural Science Foundation of Hei Long Jiang Province, the National Science Foundation with the Excellent Young Investigator Award, the National Natural Science Foundation of China and the Multidisciline Scientific Research Foundation of Harbin Institute of Technology (HIT. MD2001.39).

References

(1) Chen, Z.T., Karihaloo, B.L. and Yu, S.W., A Griffith Crack Moving Along the Interface of Dissimilar Piezoelectric Materials, Int. J. Fracture., Vol. 91 (1998), pp. 197-203.

(2) Paul, H.S. and Nelson, V.K., Axisymmetric Vibration of Piezo-composite Hollow Circular Cylinder, Acta Mech., Vol. 116 (1996), pp. 213-222.

(3) Khutoryansky, N.M. and Sosa, H., Dynamic Representation Formulas and Fundamental Solutions for Piezoelectricity, Int. J. Solids. Structures, Vol. 32 (1995), pp. 3307-3325.

(4) Shindo, Y., Katsura, H. and Yan, W., Dynamic Stress Intensity Factor of a Cracked Dielectric Medium in a Uniform Electric Field, Acta Mech., Vol. 117 (1996), pp. 1-10.

(5) Narita, K. and Shindo, Y., Scattering of Anti-plane Shear Waves by a Finite Crack in Piezoelectric Laminates, Acta Mech., Vol. 134 (1999), pp. 27-43.

(6) Chen, Z.T. and Karihaloo, B.L., Dynamic Response of a Cracked Piezoelectric Ceramic under Arbitrary Electro-mechanical Impact, Int. J. Solids. Structures, Vol. 36 (1999), pp. 5125-5133.

(7) Sosa, H. and Khutoryansky, N., Transient Dynamic Response of Piezoelectric Bodies Subjected to Internal Electric Impulses, Int. J. Solids. Structures, Vol. 36 (1999), pp. 5467-5484.

(8) Pak, Y.E., Crack Extension Force in a Piezoelectric Material, J. Appl. Mech., Vol. 57 (1990), pp. 647-653.

(9) Pak, Y.E., Linear Electro-elastic Fracture Mechanics of Piezoelectric Materials, Int. J. Fracture, Vol. 54 (1992), pp. 79-100.

(10) Suo, Z., Kuo, C.-M., Barnett, D.M. and Willis, J.R., Fracture Mechanics for Piezoelectric Ceramics, J. Mech. Phy. Solids, Vol. 40 (1992), pp. 739-765.

(11) Suo, Z., Models for Breakdown-resistant Dielectric and Ferroelectric Ceramics, J. Mech. Phy. Solids, Vol. 41 (1993), pp. 1155-1176.

(12) Park, S.B. and Sun, C.T., Effect of Electric Field on Fracture of Piezoelectric Ceramics, Int. J. Fracture, Vol. 70 (1995), pp. 203-216.

(13) Park, S.B. and Sun, C.T., Fracture Criteria for Piezoelectric Ceramics, Journal of American Ceramics Society, Vol. 78 (1995), pp. 1475-1480.

(14) Tauchert, T.R., Cylindrical Bending of Hybrid Laminates under Thermo-electro-mechanical Loading, J. Therm. Stresses, Vol. 19 (1996), p. 287.

(15) Lee, J.S. and Jiang, L.Z., Exact Electro-elastic Analysis of Piezoelectric Laminate via State

Space Approach, Int. J. Solids. Structures, Vol. 33 (1996), p. 977.
(16) Tang, Y.Y., Noor, A.K. and Xu, K., Assessment of Computational Models for Thermoelectroelastic Multilayered Plates, Comp. Struct., Vol. 61 (1996), p. 915.
(17) Batra, R.C. and Liang, X.Q., The Vibration of a Rectangular Laminated Elastic Plate with Embedded Piezoelectric Sensors and Actuators, Comp. Struct., Vol. 63 (1997), p. 203.
(18) Heyliger, P., Exact Solutions for Simply Supported Laminated Piezoelectric Plates, ASME J. Appl. Mech., Vol. 64 (1997), p. 299.
(19) Shindo, Y., Domon, W. and Narita, F., Dynamic Bending of a Symmetric Piezoelectric Laminated Plate with a through Crack, Theor. Appl. Fract. Mech., Vol. 28 (1998), p. 175.
(20) Narita, K. and Shindo, Y., Scattering of Love Waves by a Surface-breaking Crack in Piezoelectric Layered Media, JSME Int. J. Ser. A, Vol. 41, No. 1 (1998), p. 40.
(21) Narita, K., Shindo, Y. and Watanabe, K., Anti-plane Shear Crack in a Piezoelectric Layered to Dissimilar Half Spaces, JSME Int. J. Ser. A, Vol. 42, No. 1 (1999), pp. 66-72.
(22) Morse, P.M. and Feshbach, H., Methods of Theoretical Physics, Vol. 1 (1958), McGraw-Hill, New York.
(23) Han, Xue-Li and Wang, Tzuchiang, Interacting Multiple Cracks in Piezoelectric Materials, Int. J. Solids. Structures, Vol. 36 (1999), pp. 4183-4202.
(24) Deeg, W.E.F., The Analysis of Dislocation, Crack and Inclusion Problems in Piezoelectric Solids, Ph.D. Thesis, Stanford University, 1980.
(25) Sosa, H., On the Fracture Mechanics of Piezoelectric Solids, Int. J. Solids. Structures, Vol. 29 (1992), pp. 2613-2622.
(26) Zhang, T.Y. and Tong, P., Fracture Mechanics for a Mode III Crack in a Piezoelectric Material, Int. J. Solids. Structures, Vol. 33 (1996), pp. 343-359.
(27) Zhang, T.Y., Qian, C.F. and Tong, P., Linear Electro-elastic Analysis of a Cavity or a Crack in a Piezoelectric Material, Int. J. Solids. Structures, Vol. 35 (1998), pp. 2121-2149.
(28) Gao, H., Zhang, T.Y. and Tong, P., Local and Global Energy Rates for an Elastically Yielded Crack in Piezoelectric Ceramics, J. Mech. Phy. Solids., Vol. 45 (1997), pp. 491-510.
(29) Wang, B., Three Dimensional Analysis of a Flat Elliptical Crack in a Piezoelectric Materials, Int. J. Engng. Sci., Vol. 30 (1992), pp. 781-791.
(30) Narita, K. and Shindo, Y., Anti-plane Shear Crack Growth Rate of Piezoelectric Ceramic Body with Finite Width, Theor. Appl. Fract. Mech., Vol. 30 (1998), pp. 127-132.
(31) Shindo, Y., Narita, F. and Tanaka, K., Electroelastic Intensification near Anti-plane Shear Crack in Orthotropic Piezoelectric Ceramic Strip, Theor. Appl. Fract. Mech., Vol. 25 (1996), pp. 65-71.
(32) Yu, S.W. and Chen, Z.T., Transient Response of a Cracked Infinite Piezoelectric Strip under Anti-plane Impact, Fatigue and Engineering Materials and Structures, Vol. 21 (1998), pp. 1381-1388.
(33) Gradshteyn, I.S. and Ryzhik, I.M., Table of Integral, Series and Products, (1980), Academic Press, New York.
(34) Erdelyi, A.(ed.), Tables of Integral Transforms, Vol. 1 (1954), McGraw-Hill, New York.
(35) Keer, L.M. and Luong, W.C., Diffraction of Waves and Stress Intensity Factors in a Cracked Layered Composite, Journal of the Acoustical Society of America, Vol. 56 (1974), pp. 1681-1686.
(36) Amemiya, A. and Taguchi, T., Numerical Analysis and Fortran, (1969), Maruzen, Tokyo.
(37) Itou, S., Three Dimensional Waves Propagation in a Cracked Elastic Solid, ASME J. Appl. Mech., Vol. 45 (19787), pp. 807-811.
(38) Itou, S., Three Dimensional Problem of a Running Crack, Int. J. Engng. Sci., Vol. 17 (1879), pp. 59-71.
(39) Zhou, Z.G., Bai, Y.Y. and Zhang, X.W., Two Collinear Griffith Cracks Subjected to Uniform Tension in Infinitely Long Strip, Int. J. Solids. Structures, Vol. 36 (1999), pp. 5597-5609.
(40) Zhou, Z.G., Han, J.C. and Du, S.Y., Investigation of a Griffith Crack Subject to Anti-plane Shear by Using the Non-local Theory, Int. J. Solids. Structures, Vol. 36 (1999), pp. 3891-3901.